AIMS Biophysics

AIMS Biophysics, 11(1): 39−65.
DOI: 10.3934/biophy.2024004
Received: 02 November 2023
Revised: 23 December 2023
Accepted: 09 January 2024
Published: 22 January 2024

http://www.aimspress.com/journal/biophysics

Review

Computer implementation of the method for electrolytic production of thin films for biomedical applications: short review

Alexander Galashev*

Institute of High Temperature Electrochemistry, Ural Branch, Russian Academy of Sciences, Academic Str. 20, Ekaterinburg, 620066, Russia

* **Correspondence:** Email: alexander-galashev@yandex.ru; Tel: +7-343-362-3143; Fax: +7-343-374-5904.

Abstract: Optimizing the electrodeposition process condition requires considerable effort and time. The use of modeling and simulations can largely solve this problem. This short review is focused on the development of mathematical models and molecular dynamics simulations, which can be used to predict the electrodeposition of thin silicon and silicon carbide films using the KCl-KF-KI electrolyte. The use of computer simulations to obtain thin films of silicon nitride and silicon dioxide is considered. Silicon, silicon dioxide, silicon nitride, and silicon carbide are important biomedical materials. Additionally, we consider modeling the decomposition process of various precursors used as sources of Si^{4+} and C^{4+} ions for electrolytic deposition. The calculation of various physical properties of crystalline silicon and important modifications of silicon carbide, including the thermal conductivity, surface diffusion coefficients, and a detailed structure determined by constructing Voronoi polyhedra, are discussed. A computer model allows one to explore the use of "a defective silicene/silicon carbide" hybrid material as a lithium-ion battery anode. The possibilities for solving problems of processes optimization in modern methods for producing biomedical materials are discussed.

Keywords: diffusion; electrolytic deposition; film; ion; molecular dynamics; molten salt; silicon; silicon carbide; structure; Voronoi polyhedra

1. Introduction

Both silicon (Si) and silicon carbide (SiC) are biomaterials widely used in medicine. First, let us

exemplify the use of silicon, and then the use of silicon carbide for these purposes. Si has a fairly high biocompatibility and biostability when introduced into living tissues. Si is hydrophobic and has low surface tension, which leads to a high hemocompatibility. There is a low likelihood of silicon forming a crust upon contact with various body fluids [1]. At the same time, the chemical and thermal stability of Si often makes it possible to avoid repeated sterilization, because the impact of host tissues is small. Due to these properties, Si materials are widely used in biomedicine. Tubes for catheters and drainages are made from silicon elastomer. Typically, electronic implants are silicon insulated. Due to air permeability, silicon adhesives are used when bandaging wounds, and prosthetic parts are made of silicon rubber [2]. Moreover, various "long-lasting" implants, such as orthopedic and aesthetic implants, are still made from Si [3].

At first, Si was the best material among semiconductors for biotechnological applications. It has been used as a substrate material for microdevices due to its low cost and availability. Gradually, a number of disadvantages were discovered when using this material for biomedical purposes. In particular, Si was found to have a low rate of interaction with the body and a short period of stability when used in vivo. Ultimately, a more effective material that had the ability not to be rejected by the body and would not be recognized as a foreign body was needed [4]. It turned out that silicon carbide largely satisfies these requirements [5].

Finally, silicone elastomer is widely used as a material in maxillofacial prosthetics [6]. It is flexible, heat resistant, transparent, and biocompatible. The chemical structure of silicone consists of an inorganic backbone composed of alternating Si and oxygen atoms. Organic side groups are attached to this siloxane structure. Mechanical properties of silicone are determined by the molecular weight, the degree of cross-linking, and the inclusion of fillers and pigments.

Still, Si is mainly used in electronics. As a semiconductor, Si is used in devices such as transistors, printed circuit boards, and integrated circuits. To improve the performance in most electronic applications, these semiconductors are doped to increase the conductivity and to make the device more stable.

Crystalline SiC is a semiconductor material that is extremely attractive for bioapplications [7]. All major SiC polytypes directly interact with cells in vitro and in the absence of a specific surface functionalization. In addition, doping with SiC does not significantly affect the biocompatibility of this material [8]. The biocompatibility of SiC is mainly determined by its excellent tribological properties, hydrophilicity, and surface chemistry. Crystalline Si (3C-SiC) shows a certain degree of biological activity when interacting with connective tissue cells. Tests have shown the applicability of amorphous SiC (a-SiC) and 3C-SiC in neural probes [4]. In the presence of a dense vascular network in the brain, the hemocompatibility of implanted biodevices comes to the fore (i.e., neural implants).

The widespread use of electrochemical biosensors in clinical practice and healthcare, especially in multiplex assays, is due to their high sensitivity, low cost, and small size [9]. The multiplex electrochemical biosensors functioning on Si and SiC bases provide promising results. This is confirmed by precise multiplexing for early diagnoses and monitoring of progressive diseases. Improving the design of electrochemical devices makes them more sensitive and compact. Computer modeling makes an invaluable contribution to their further improvement.

Silicon carbide serves as the best material for mirror optics. Hardness, rigidity, mechanical stability, and a reasonable density allow SiC to be used to manufacture the space optical devices [10]. Silicon carbide can be produced in different ways; however, for each methodology, it is difficult to obtain a high-quality optical surface, and bare SiC polishing is very difficult. Furthermore,

microstructural defects such as pores, steps in different phases, and damage to the grain boundaries also make polishing difficult. As a result, manufacturing high-precision optical components from SiC is an expensive and slow process.

Silicon carbide can be used in harsh environments due to its strength and excellent mechanical properties [11]. Solar radiation received by the Earth is 10,000 times higher than global energy needs [12]. Cubic silicon carbide (3C-SiC) is of great interest in solar cell technology, where it is used as a top protective layer [13,14]. Amorphous SiC_x films with a high silicon content are often utilized as transparent layers of solar cells. Films with a high carbon content are suitable as an active layer in electroluminescent devices [15].

The analytical design of thin film electrodes requires knowledge of the charge and mass transfer processes, including kinetic characteristics, alongside data on the detailed structure of the electrode being modeled. For example, in the continuum model, it is difficult solve the problem of oxygen reduction on the porous cathode of a solid-state oxide fuel cell of mixed conductivity [16]. The aim of modeling processes for obtaining pure Si and SiC is to establish the underlying microscopic mechanisms and to determine the influence of process parameters such as pressure, temperature, etc., on the resulting atomistic structure and kinetics. The physical vapor deposition of 4H or 6H-SiC polytype during SiC crystal growth is an example of this kind of simulation [17].

Silicon nitride (SiN_x) is a promising material for biomedical applications. This material has a good biocompatibility, chemical inertness, high fracture toughness, and high wear resistance [18]. SiN_x films can be used as thin viewing windows for biomedical microdevices [19]. They are suitable for isolation membranes of cell electroporation and gene transfection [20]. Additionally, SiN_x membranes are used for protein filtration and in vitro models of the blood-brain barrier. Compared to polymer membranes, SiN_x membranes have sufficient mechanical strength, precisely controlled pore characteristics, and are not susceptible to morphological changes or degradation in biological fluids. An SiN_x film is the original material to manufacture selective emitter solar cells [21]. Phosphorus-doped SiN_x and SiN(P) layers both have excellent anti-reflection and passivation properties. SiN(P) is used as a solar cell material due to the ability of this material layer to simultaneously act as an antireflection coating, a passivation layer, and a one-sided dopant source [22]. Phosphorus-doped SiN_x nanoparticles are considered as a promising biomedical platform, with a great impact in the treatment and diagnosis of diseases. However, clinical translation and commercialization of the SiN(P) fine materials can only be achieved through the development of standardized and unified biological evaluation methods.

Silicon dioxide (SiO_2) ultra-thin oxide films are excellent components for modern nanotechnologies. They are used in silicon microelectronic devices, anticorrosion films, and in catalysis [23]. Silica (SiO_2)-composite nanoparticles provide reliable support for the immobilization of various biomolecules. With their use in immunoassays, highly selective and sensitive procedures can be performed, thus taking advantage of the specific interactions between antigen and antibody [24]. In recent years, the method of electrodeposition (i.e., producing coatings by exposure to electric current) has become increasingly popular. This is largely due to its ability to create three-, two-, and one-dimensional nanostructures. In particular, nanotubes, nanowires, and nanorods can be obtained in this way [25].

Electrodeposition is one of the most inexpensive methods to produce thin films of metals, metal alloys, and compounds. It is a nonvacuum, large industrial scale-based deposition technique and energy efficient process that is usually carried out at low (close to room) temperatures. With a properly

selected electrolyte, an almost 100% utilization of materials is achieved during the electrodeposition. In this method, multiple deposition parameters can individually and jointly influence the properties of the resulting material. However, in some cases, by adjusting the current density, it is easy to control the grain size, crystallinity (or lack thereof), and mixing to obtain the desired alloys. By optimizing the electrodeposition parameters, it is possible to improve the stoichiometry of the resulting Si and SiC films, which is one of the most important properties of a semiconductor and it is critical to obtain the desired bandgap and performance. However, the correct adjustment is achieved with a deep understanding of the electrodeposition process, which can be achieved by modeling this process at the atomic level. Such simulations have been performed to clarify the details of a number of other deposition and consolidation techniques, such as chemical vapor deposition (CVD) and sintering [26–29]. However, the electrolytic deposition method has long been neglected by computer modeling. Only recently (since 2021) has this drawback been eliminated to a certain extent through our efforts.

This brief review focuses on recent molecular dynamics studies on the initial stage of electrodeposition. However, we are not limited to describing models of the electrolytic deposition process, but also present modeling of the production of thin films by some other methods.

2. Molecular dynamics models of electrolytic deposition

Let us briefly consider the molecular dynamics (MD) model to produce thin films of silicon and silicon carbide by electrolytic deposition as the cheapest and most well-regulated process [30,31]. The work [30] presented modeling of the initial growth stages of a silicon film deposited from the KF-KCl-KI melt on Ag (001) and graphite substrates. The KF-KCl-KI melt of the (19.2-9.6-71.2) mol % composition was created by melting the corresponding crystals (KF, KCl and KI). The initial configuration of the simulated system is presented in Figure 1. The thickness of the graphene and silver substrates for the deposition of silicon atoms was four and five layers of atoms, respectively.

A simplified method was used to present the appearance of Si atoms in the melt. Charged Si^{4+} ions were periodically introduced through the upper boundary of the MD cell. The introduced Si^{4+} ions had random x, y coordinates and a constant z coordinate, which determined the position of the ion above the surface of the molten salt. Silicon ions were deposited on the bottom of the cell (substrate) under the influence of an electric field, $E=10^4$ V/m. When they reached the negative electrode (substrate), the deposited ions turned into neutral atoms, which were no longer affected by the electric field. The silicon deposition process was carried out in an *NVT* ensemble at a temperature of 1000 K, which is close to the temperature of the real electrolytic process, which takes place in the range from 993 to 998 K [32].

The interaction between the particles in the melt was described by a hybrid potential, including Coulomb and Lennard-Jones contributions [31]. The Lennard-Jones potential is the most commonly used non-bonded potential. Essentially, this potential is analogous to the van der Waals force of interaction. The potential has both a repulsive contribution ($\sim 1/r^{12}$) and an attractive contribution ($\sim 1/r^6$). The first part of the potential explains the short-range overlap of electronic orbitals, and the second part characterizes the action of long-range intermolecular forces. Another uncoupled interaction is the electrostatic interaction, which is expressed through the Coulomb forces. To model electrostatic interactions, it is assumed that atoms can be treated as point charges by assigning each atom its corresponding electrical charge. When calculating the energy of a periodic system of charged particles, a special type of summation is required (e.g., Evald summation (with transition to reciprocal space)) [33].

However, in works related to electrodeposition modeling, the particle-particle-particle mesh (PPPM) summation method was used [34]. It uses the 3D fast Fourier transform to solve Poisson's equation on a grid. This is a significantly faster summation method than the Ewald method.

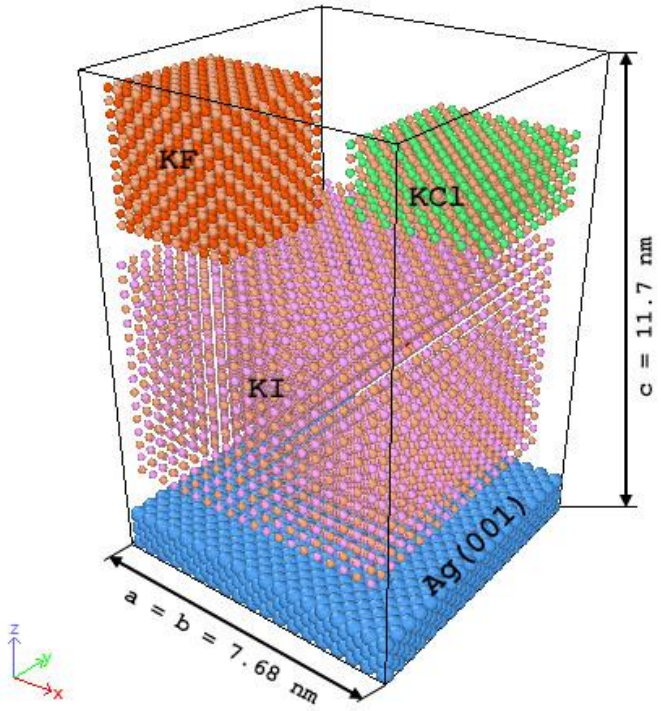

Figure 1. General view of the original system at time t = 0 ns [30]. The system dimensions are as follows: a = b = 7.68 nm, c= 11.7 nm.

Silicon ions interact with the substrate according to the Morse potential [35]. This potential poses fewer problems with the cutoff distance, as compared with the LJ potential, because its potential curve has a faster decay. The Morse potential has three parameters characterizing the binding energy, the periodicity of the corresponding crystal lattice, and the bulk modulus. The interaction between silver atoms in the substrate was described by the embedded atom model (EAM) potential [36], while the interaction between carbon atoms in the graphite substrate was a subject of the Tersoff potential [37]. The force-matching method allows one to construct a physically based interparticle EAM potential without resorting to experimental data [38]. The construction of this potential is done by an ab initio calculation of interactions in a finely tuned set of small reference structures. The final step in this calculation is to tune the interparticle potential to optimally reproduce the forces acting on the atom. The EAM potential is widely used to describe atomic interactions in metals and alloys. The Tersoff potential is commonly used to model materials such as Si, Ge, C, and alloys of these materials. Using this potential, the total binding energy of the system is determined, which is the sum of the binding energy of each bond. When determining the energy of an individual bond, the pairwise repulsive and attractive contributions are taken into account. The calculation of attractive energy involves determining the bond order, which takes the local coordination number and bond angles into account. Multiplying the bond order by the bond energy gives the attractive energy. The local coordination number is an important element of the Tersoff potential. It allows either linear, trigonal, or tetrahedral

geometry to be taken into account in the arrangement of covalently bonded atoms. This potential has a two-particle form of representation, in which the two-particle terms depend on the local environment.

The basic operations for the salt melt preparation and ions deposition described in [30] and [31] were identical; however, when growing a silicon carbide film through the top of the MD cells, two types of ions, Si^{4+} and C^{4+}, were periodically introduced into the molten salt mixture. Due to the short time of observation of the system during the computer simulation in relation to the time of a real experiment, it becomes necessary to alternately introduce ions into the model volume to form a precipitate. Otherwise, Si^{4+} ions can accumulate in the volume of the model melt and form clusters, which will lead to the formation of a Si film on the substrate impossible. The time interval for Si^{4+} ions introduction into the melt was empirically selected. The authors of [30] note that this time (30 ps) significantly exceeds the time (ranging from 1 to 10 ps) during which the Si^{4+} ion, having reached the substrate, will occupy an energetically favorable place on it. Additionally, the time intervals to introduce Si^{4+} and C^{4+} ions into a molten salt located under an external electric field were empirically selected to obtain a fairly uniform silicon carbide film on the substrate [31]. Moreover, the selected time intervals for launching Si^{4+} (30 ps) and C^{4+} (50 ps) ions eliminated the problem of cluster formation in the volume of the molten salt. A diagram of the process of silicon and carbon ions co-deposition is shown in Figure 2.

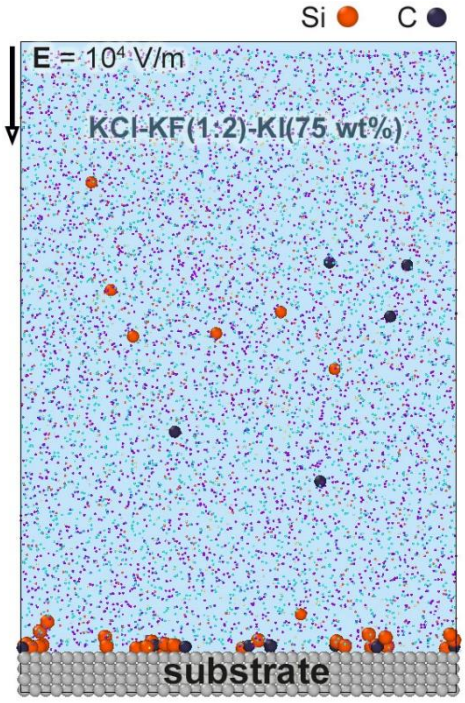

Figure 2. Schematic representation of the Si^{4+} and C^{4+} deposition process from the melt to the substrate [31]. Silicon and carbon ions were introduced in the system periodically, the particles moved through the melt into the substrate direction under the action of the electrical field E.

In [30,31], a statistical analysis of the structure obtained in the model of Si and SiC thin films electrolytic deposition was performed on the basis of the Voronoi polyhedra (VP) construction [39–41]. Silicene, which was located on identical substrates with Si films, was subjected to the same structural

studies. In both cases, it is possible to construct three-dimensional VPs, because the systems under consideration are not absolutely flat. However, such VPs do not have a high degree of symmetry. Studying the structure of the system using VP turns out to be preferable when compared to constructing the radial distribution function, because it reveals the three-dimensional structure in detail.

The diagram for constructing a Voronoi polyhedron is shown in Figure 3. A detailed description of the image is presented below. The atoms in Figure 3 are represented by dots, and the circles around the dots represent the central atom and its nearest geometric neighbors. The proposed geometric neighbors are enclosed within a large circle drawn from the selected center. Cutting off extra atoms speeds up the VP construction procedure during modeling. The bold lines show the VP faces and perpendiculars are drawn from the central atom to its geometric neighbors. Some of the faces formed by second-order neighbors are displayed by dotted lines, which are perpendicular to the straight segments connecting the selected center with the corresponding neighbors. All faces pass through the midpoints of the segments connecting the central atom with its neighbors, both of the first and second orders.

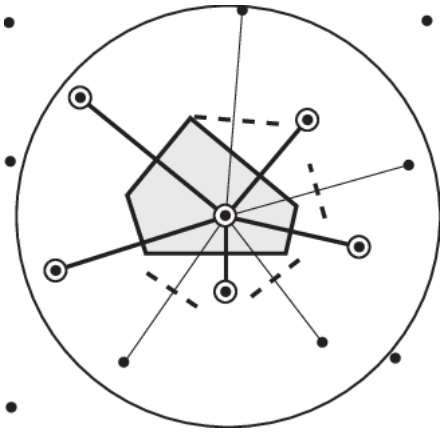

Figure 3. Schematic for constructing Voronoi polyhedra in the two-dimensional case.

Voronoi polyhedra are constructed through a certain number of time steps. In [30,31,39–41], due to the smallness of the used time step dt (1 fs), the interval for constructing VPs was a time interval equal to 1000 Δt. This excluded the possibility of including the statistical analyses of almost identical atomic configurations that appear during the construction of VPs at each very small time step. The object of the statistical analysis is the elements of the Voronoi polyhedra, among which the number of faces, the number of sides in a face, the angles formed by straight segments passing through the center VP, and all pairs of the nearest geometric neighbors (i.e., those neighbors whose presence leads to the formation of faces in the VP under consideration).

The distribution of polyhedra by the number of faces shows the probability of occurrence of a certain number of the nearest geometric neighbors surrounding the atoms in the system and the correlation of these probability numbers. The distribution of faces by the number of sides has a similar physical meaning. However, in this case, the role of polyhedra is played by their faces, and the role of faces is played by the sides in these faces. However, there is another interpretation of the physical meaning of the distribution of faces by the number of sides. According to this interpretation, the physical meaning of this distribution is that the probability of observing cyclic formations (rings

created by geometric neighbors) having a given number of links from the center VP is determined. Moreover, an observation is carried out in all directions, as determined by lines connecting the selected center (observation location) with the corresponding geometric neighbors. Finally, the angular distribution shows the probability of observing angles formed by pairs of the nearest geometric neighbors and the central atom - the vertex of the angle. In other words, this distribution represents the frequency of occurrence of viewing angles when observing all pairs of the nearest geometric neighbors from the VP center.

3. Modeling the production and calculation of the properties of crystalline and amorphous silicon carbides

Atomic layer deposition mechanisms of CVD SiC were investigated by the ab initio simulation using the VASP software package [42]. The reaction energetics and decomposition progress of various Si and C precursors were analyzed using the plasma activation of particles on bare and H-terminal 3C-SiC (011) surfaces. Silicon tetrachloride ($SiCl_4$), disilane (Si_2H_6), silane (SiH_4), trichloromethane ($CHCl_3$), propine (C_3H_4), ethylene (C_2H_2), and carbon tetrachloride (CCl_4) were used as Si and C precursors. In addition, plasma components of silyl (SiH_3) and silylene (SiH_2) were also involved. All Si and C sources under consideration interacted with the surfaces under consideration in a similar manner: they exhibited reactions with the H-terminal groups on the SiC surface and spontaneously interacted with the corresponding bare surface. The conditions for the layer-by-layer growth of a SiC film were formulated in the following form: first, a C source was introduced (pulsed) to react with the bare surface of the SiC substrate; then, a Si source was introduced (pulsed). After these actions, plasma particles were activated; these particles selectively reacted with the Si–H surface areas and form a SiC layer. However, it is not clear whether such a mechanism will work for chemical compounds other than those considered in this work - sources of Si and C.

Based on the simulation of the 3C-SiC system, the adequacy of the computer model constructed using the density functional theory (DFT) was verified in [43]. The dependence of the properties of this system on high compression and temperature was investigated. The simulation was performed using the software package for the ab initio study (ABINIT) based on the pseudo-potential plane-wave (PP-PW) method. Using the FHI98PP program, norm-preserving Trulier-Martens pseudopotentials were obtained, and the generalized gradient approximation (GGA) i.e. the Perdew–Burke–Ernzerhof approximation was used to take the exchange-correlation interaction into account. The physical parameters calculated in this work (i.e., the melting point, the Debye temperature, the Knoop microhardness, and the thermal conductivity) were in a good agreement with the experimental data.

The influence of the mass density and the coordination of atoms on the fundamental vibrational characteristics and thermal conductivity of the a-SiC:H system was studied in [44]. This work involved MD calculations, lattice dynamics calculations, and an infrared spectroscopy apparatus. These studies concluded that the mass density and the coordination number have a strong influence on the a-SiC:H thermal conductivity obtained in the MD model. With an increasing atomic density, the median coordination of atoms increases, and the thermal conductivity of the system increases linearly (Figure 4). The similar behavior of the experimental and calculated thermal conductivities with an increasing atomic density suggests that the heat transfer mechanisms in the model are similar to those in the real systems. The authors believe that a potential mechanism for controlling thermal conductivity is possible for the a-SiC:H system.

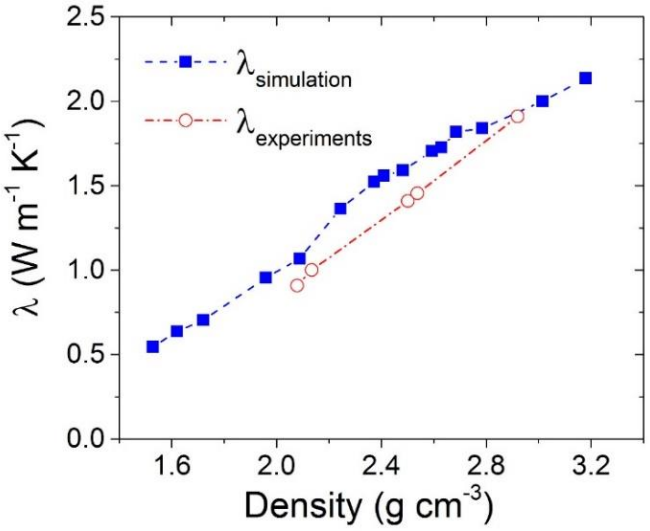

Figure 4. Dependence of the a-SiC:H thermal conductivity on atomic density. Both experimental and model data are taken from [44].

4. Simulation of electrolytic deposition of silicon film

Films of pure crystalline silicon were experimentally obtained by the electrolysis from the KF-KCl (2: 1)—75 mol% KI—0.5 mol% K_2SiF_6 melt under galvanostatic conditions on copper [45], tungsten, and glassy carbon [32] substrates. The authors [32] note that a high concentration of potassium iodide (from 75 to 85 mol%) promotes the formation of thin silicon films. The spread of film thickness in different parts of the electrode ranged from 452 to 800 nm, which is due to an uneven distribution of the current density over the electrode area. MD calculations confirmed the possibility of obtaining a pure silicon film by electrolysis from the melt of a similar composition: KF (19.2 mol%), KCl (9.6 mol%), KI (71.2 mol%). In the model, electrodeposition was performed on both silver and graphite substrates. To increase the rate of precipitation in the model, Si^{4+} ions were introduced periodically into the system, rather than appearing in it via the K_2SiF_6 additive dissolution.

A modeling study on the silicon films electrolytic deposition showed that the growth mechanism of the silicon film largely depends on the type of substrate used [30]. The strong interaction between Si^{4+} ions with the Ag (001) substrate creates conditions for the growth of several silicon clusters at once. The growth of a Si film on an Ag (001) substrate occurs due to an increase in the size of individual nucleated clusters and due to their merging. A similar growth mechanism was observed when growing silicene on a metal substrate [46]. In the case of an Ag (001) substrate, it is filled layer-by-layer with silicon (Figure 5a).

The silicon film on a graphite substrate has a block structure. Moreover, blocks with a hexagonal structure have different orientations (Figure 5b). The growth of a silicon film on a graphite substrate occurs due to the gradual increase in the size of one initially nucleated cluster. This is due to the fact that the graphene surface appears to have a hexagonal honeycomb structure, which initiates the formation of a local hexagonal packing of Si atoms on its surface. However, the mismatch of lattice periods of graphene and silicene only leads to a local hexagonal arrangement of Si atoms on the surface of the substrate. On a graphite substrate, subsequent layers of silicon begin to grow when the previous layer has not yet been completely filled. This is due to a weak interaction of the film with the graphite

substrate. This is what causes the sp^3 hybridization, thus leading to the appearance of multilayer islands on the graphite surface.

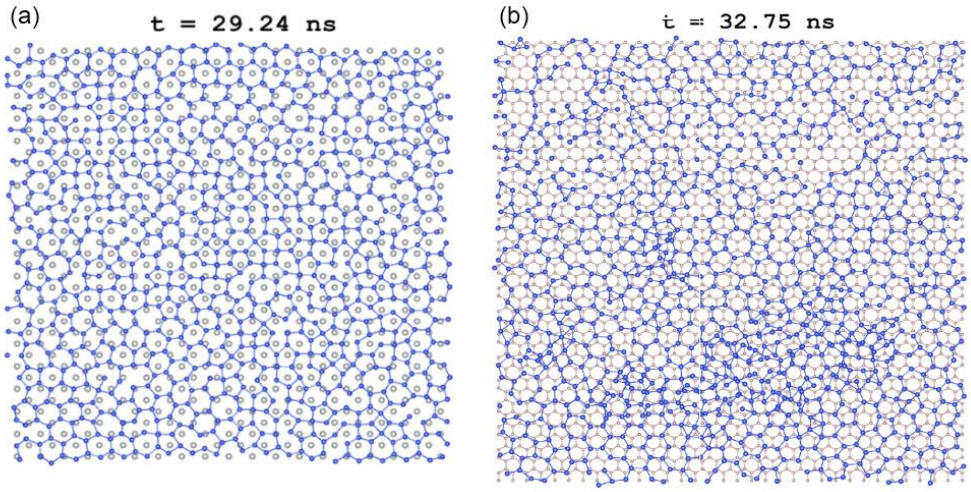

Figure 5. Two-dimensional silicon films grown on (a) silver and (b) graphite substrates in the KF-KCl-KI melt (Si atoms in blue) [30]. The time points, to which the configurations relate, are indicated in the Figure.

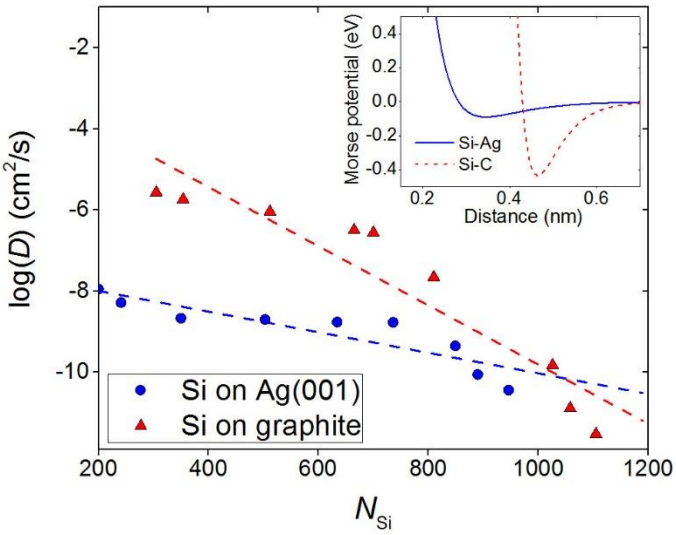

Figure 6. Surface diffusion of silicon atoms on silver (in blue) and graphite (in red) surfaces, dashed lines show a linear approximation of the dependencies [30]. The inset shows the form of the Morse potential as a function of interatomic distance; Si-Ag interaction is presented in blue, Si-C interaction is presented in red.

The low adhesion value of the Si/graphite system results in the higher surface diffusion of Si atoms on the surface of the graphite substrate as compared to that on the silver substrate (Figure 6). An insert in Figure 6 reflects the Morse potentials describing the Si-Ag and Si-C interactions. The displacement of the potential well towards larger distances significantly reduces the adhesion of the

Si/graphite system.

Single-layer silicon films were grown both on silver and on graphite substrates. The proximity of these structures to silicene was established by constructing Voronoi polyhedra. Figure 7 compares the VP distributions to the number of faces (*n* distributions) for two silicon films. One of them was obtained in the electrolytic deposition model, and the other appeared to be silicene, when both two-dimensional structures were located on identical substrates (silver and graphite). Films of approximately the same size were considered. The constructed *n* distributions, as well as the distributions of faces by the number of sides (*m* distributions), showed that the structure of the Si film on graphite was more consistent with silicene (on graphite) than the structure of the film obtained on the Ag (001) substrate when silicene is located on a silver surface.

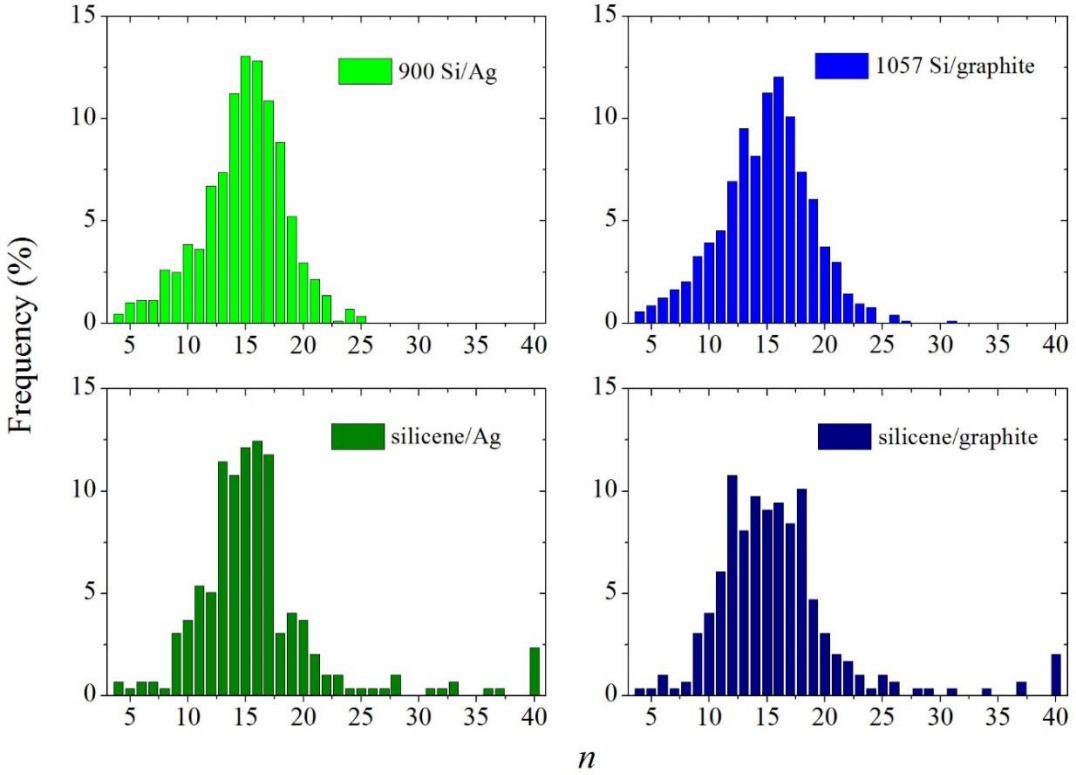

Figure 7. Distribution of Voronoi polyhedra by the number of faces for a single-layer silicon film deposited on the Ag (001) and graphite substrates (the number in the legend shows the number of deposited Si atoms), and for silicene posted on the corresponding substrates [30].

5. Modeling of the electrolytic deposition of a silicon carbide film

MD modeling of the electrolytic deposition of a silicon carbide film on Ni (001), Cu (001), and graphite substrates was performed in [31]. The formation mechanisms of SiC films on metal and graphite turned out to be similar to the formation mechanisms of Si films on silver and graphite, which was considered in [30]. On a metal surface, the formation of a SiC film predominantly occurred by the layer-by-layer growth mechanism; the growth of subsequent layers of the SiC film on a graphite

surface began much earlier than the formation of the single-layer film which completely covered the entire area of the substrate. In other words, the vertical growth of SiC on graphite competed with the layer-by-layer growth of the film. The films obtained in [31] are shown in Figure 8. In the case of a metal substrate, islands were formed on the substrate surface not occupied by the film, which were gradually tightened due to the attachment of newly deposited Si and C atoms. When the single-layer film has not yet completely covered the surface of the graphite substrate, an active and mobile growth center appeared on it, which joins the newly arriving material in the form of Si atoms and C. Here, there was competition between the sp^3 and sp^2 hybridizations.

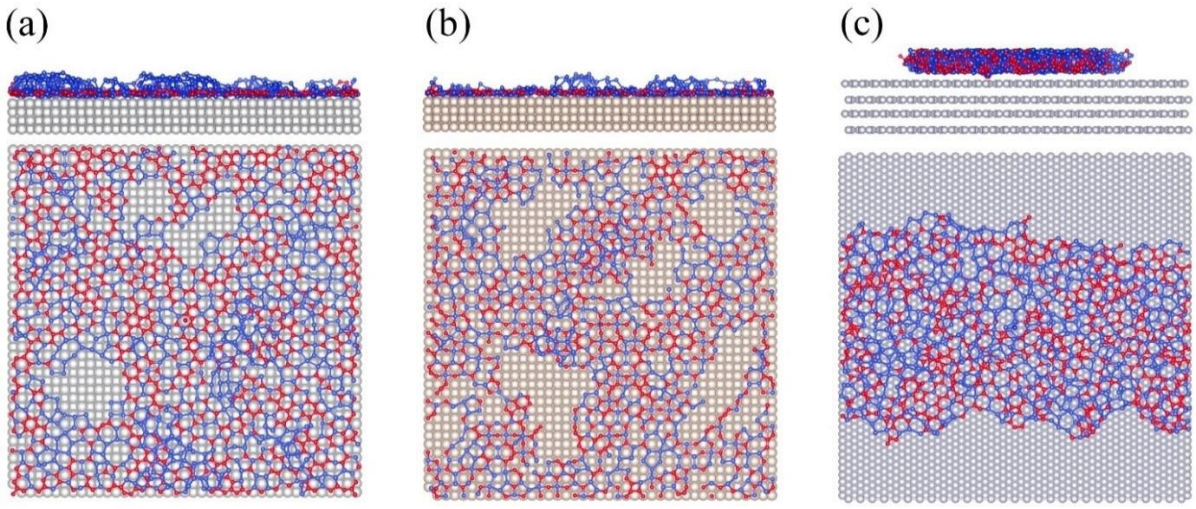

Figure 8. *xy*-projections of deposited SiC films on (a) nickel, (b) copper, (c) graphite substrates. In the case of metal substrates, the simulation time is ≈60 ns, in the case of graphite, ≈50 ns [31]. Carbon atoms are marked in red; silicon atoms are marked in blue.

Surface self-diffusion coefficient *D* of C and Si atoms depending on the total number of atoms on the substrates are presented in Figure 9. As can be seen, the coefficient *D* decreases as the substrate is filled with Si and C atoms. Lighter C atoms are always more mobile than Si atoms.

The degree of crystallinity of the resulting film was determined from the angular distributions of the nearest geometric neighbors constructed using VPs. A regular distribution of peaks in the angular distribution indicates the crystallinity of the resulting film. Figure 10 shows the statistical angular characteristics for both the subsystems of the individual components (Si and C) and the entire system (SiC) as a whole. It can be seen that the SiC film grown on graphite has a higher degree of crystallinity than the corresponding film grown on metal surfaces. At the same time, the film on a copper substrate is more crystalline than the film on a nickel substrate. The established patterns apply to both the entire SiC film and to its individual components (Si and C).

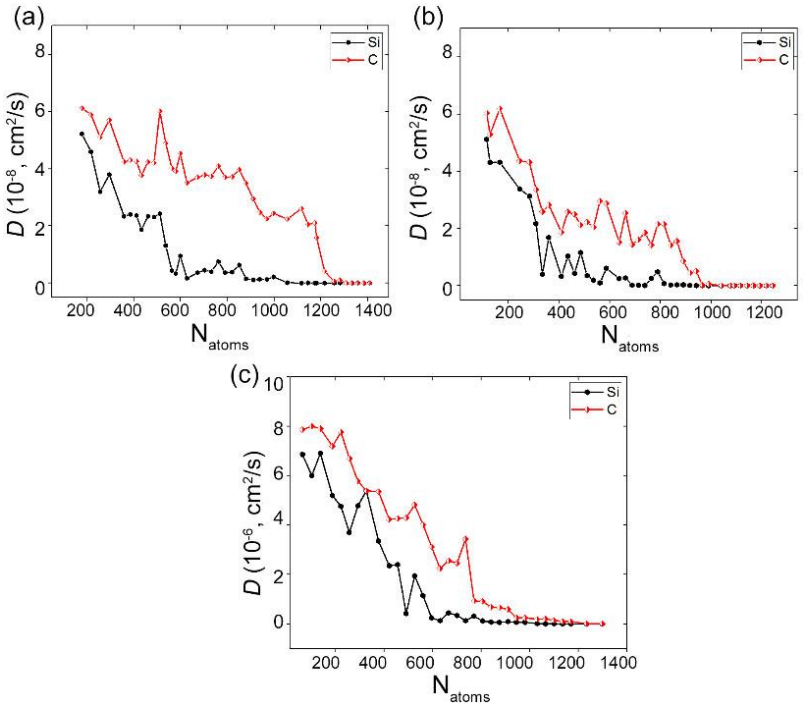

Figure 9. Surface diffusion *D* of Si (in red) and C (in black) depending on the total number of atoms on the Ni (001) (a), Cu (001) (b), graphite (c) substrates [31].

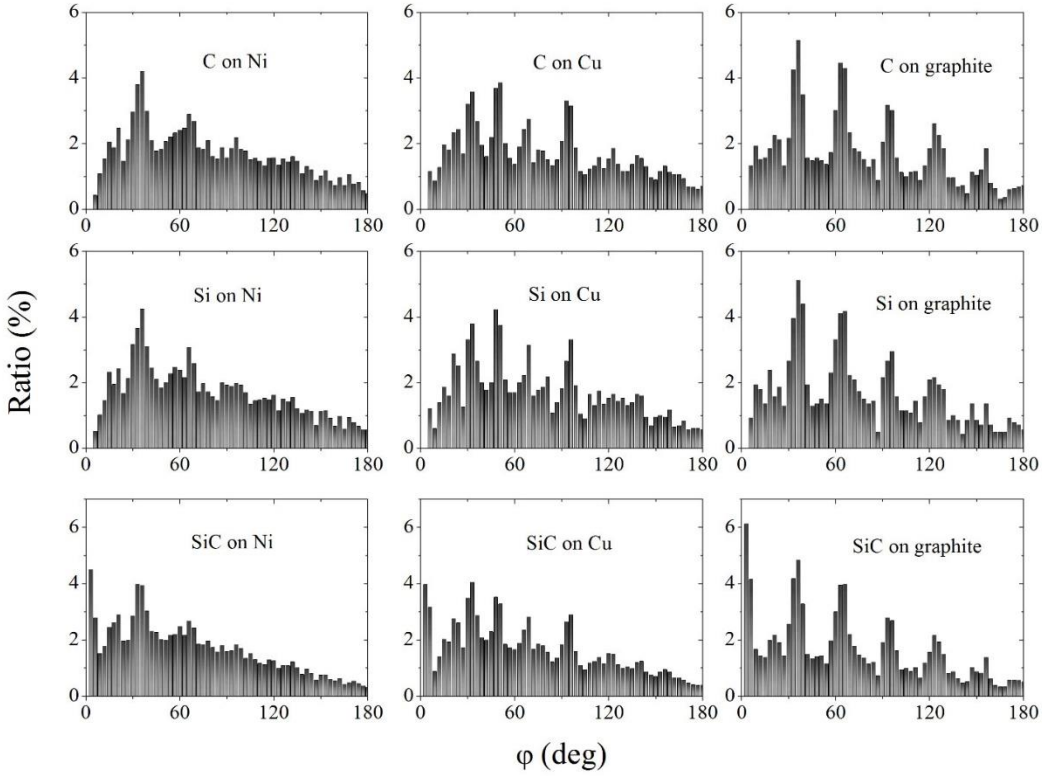

Figure 10. Angular distribution of the nearest geometric neighbors for C and Si subsystems of silicon carbide films and SiC systems as a whole, obtained on Ni, Cu, and graphite substrates [31].

The role of potential interactions during the growth of SiC on a graphite substrate was considered in [47]. When a SiC film is formed on a graphite surface, it would seem natural to use the many-particle Tersoff potential to describe the film-substrate interaction. However, the Tersoff potential is short-ranged. It is trimmed at the distances of 3 to 4 Å. At the same time, both the growing film and the substrate may contain defects. In the presence of defects, it is more expedient to use the Morse potential, which is cut off at a significantly larger distance (~10 Å). However, in this case, many-particle effects are not taken into account. In [47], MD modeling of the electrolytic deposition of a SiC film on a graphite substrate was performed, and the film-substrate interaction was described by both the Tersoff potential and the Morse potential.

The difference in the description of the film-substrate interaction led to differences in the adhesion values E_{ad} between the film and the substrate. Using the Tersoff potential at certain values of the number of the deposited atoms (Si and C) caused the adhesion energy to decrease by almost 50% (Figure 11). A sharp decrease in the adhesion energy in the presence of more than 750 particles in the system when using the Morse potential is due to the fact that individual clusters "merge" into a single SiC film. When the number of deposited Si and C particles becomes 1100, the adhesion energies determined at two different potentials become equal.

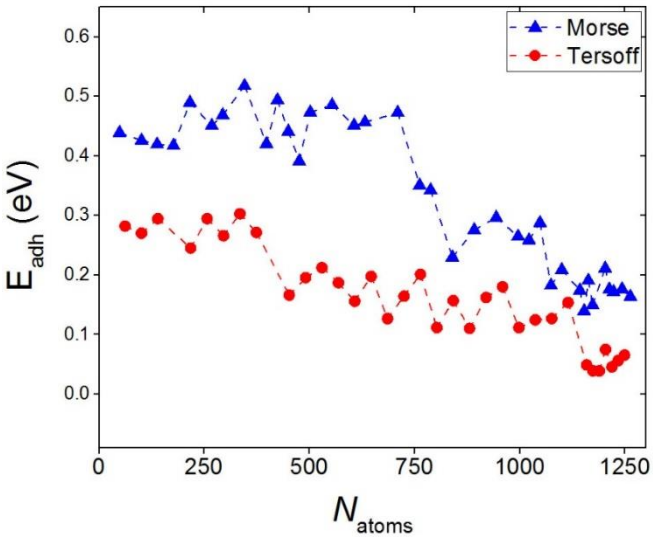

Figure 11. Adhesion energy between SiC films and a graphite substrate as a function of the total number of silicon and carbon atoms on the substrate surface; the values are given for the cases when the "film-substrate" interaction was described by the Morse potential (marked in blue) and the Tersoff potential (marked in red) [47].

The use of the Morse potential to describe the film-substrate interaction leads to a decrease in the self-diffusion coefficient of Si atoms on the surface of the graphite substrate (Figure 12). When compared to the use of a Tersoff potential, there is a ~10% decrease of D when there are Si atoms on the substrate in the amount of $N_{Si} < 650$. Moreover, the difference becomes even more pronounced (up to 30−35%) at $N_{Si} > 650$.

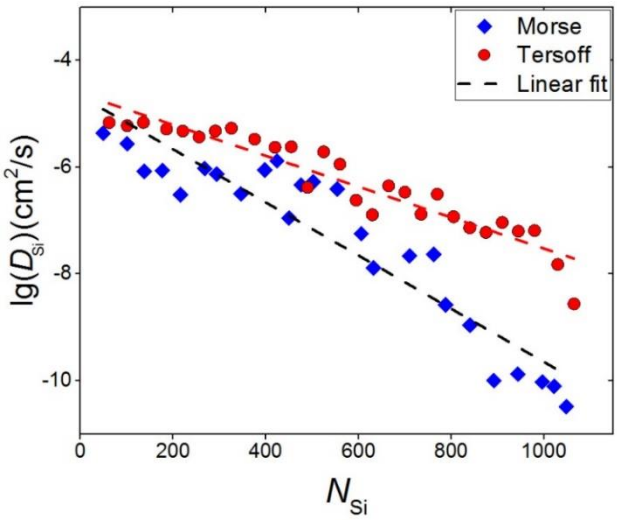

Figure 12. Surface diffusion of Si atoms as a function of the number of Si particles located on the graphite substrate; dependences (in a logarithmic scale) are shown for the case of describing the "film-substrate" interaction by the Morse potential (marked in blue) and the Tersoff potential (marked in red) [47].

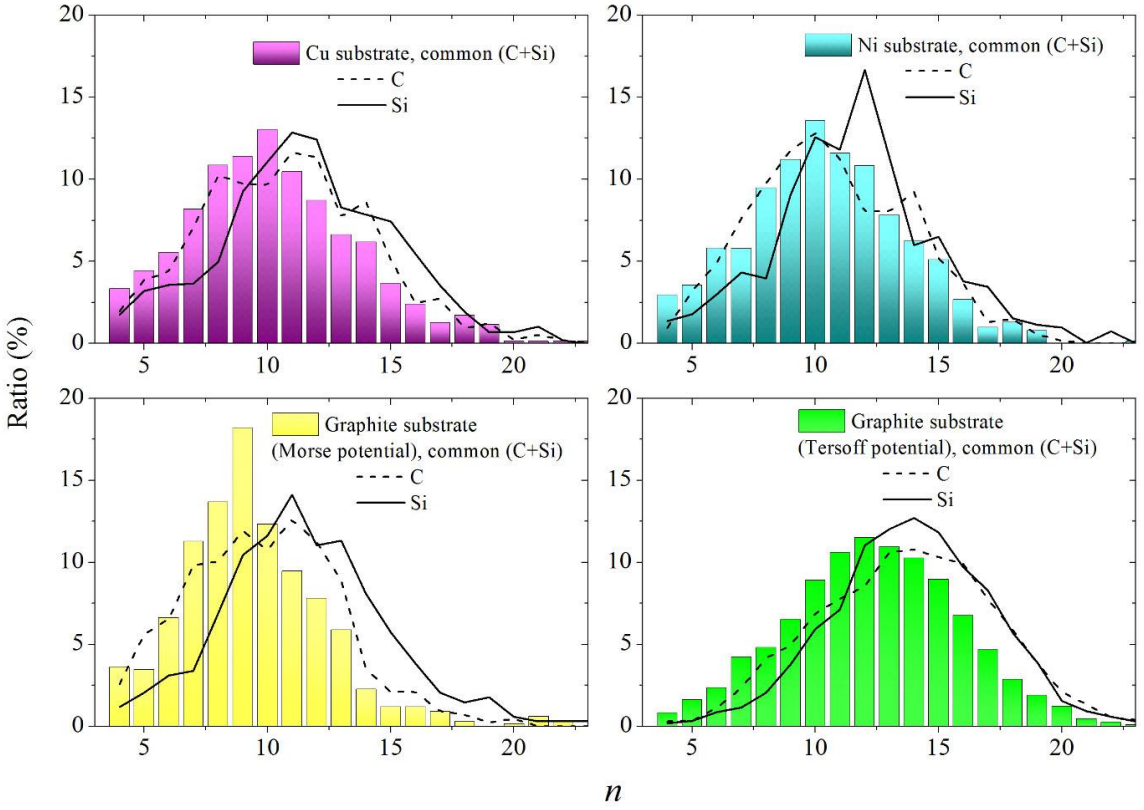

Figure 13. Distributions of Voronoi polyhedra over the number of faces obtained at the final stage of deposition of the SiC film on various substrates, both for the entire SiC film and for its individual components (C and Si); the interaction between Si or C atoms and a graphite substrate was carried out using Morse and Tersoff potentials [47].

The structure of the resulting SiC films was analyzed by constructing Voronoi polyhedra. In the case of metal substrates, the distribution maximum of VP by the number of faces occurs at $n = 10$ (Figure 13). When the substrate is graphite, the n distributions obtained when describing the film-substrate interaction by the Morse and Tersoff potentials differ significantly. When using the Morse potential, the maximum of the distribution occurs at $n = 9$; when the interaction is described by the Tersoff potential, the maximum corresponds to the value $n = 12$. In addition, in the first case, the n distribution has less dispersion than in the second case. In all cases, the maxima of the n distributions for the subsystems (Si and C) are shifted to the right relative to the corresponding distributions for the entire (SiC) system. This is due to the inclusion of Si-C bonds for the SiC system.

6. Modeling the functioning of a silicene/silicon carbide anode

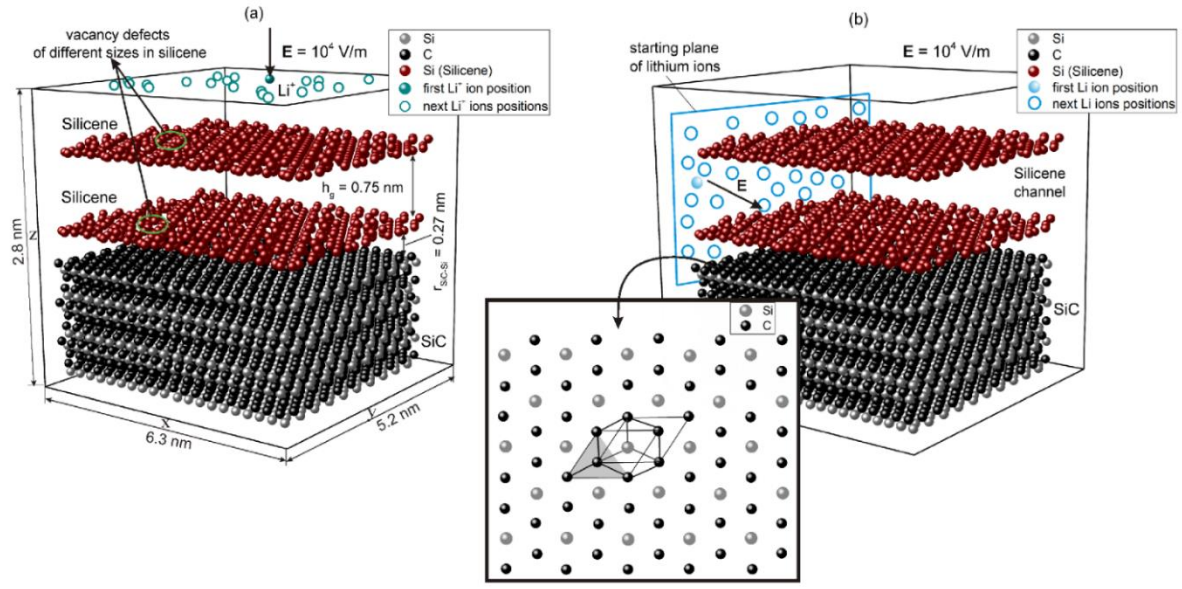

Figure 14. Schematic representation of the initial configurations (time moment t = 0 ps) of the simulated systems in the case of (a) vertical and (b) horizontal filling of the silicene channel with lithium ions; the silicene sheets have vacancies of given sizes; the ions initial sites (open circles) belongs to (a) *xy* and (b) *zy* surfaces; the insert shows a part of the substrate upper layer and a unit cell [48].

Silicon carbide film has been proposed to create a hybrid material, which could be used for the creation of new generation lithium-ion batteries (LIBs) [48]. The applicability of a hybrid material was obtained by combining a thin SiC film with a bilayer silicene as an anode material for LIBs, as studied in [49]. The use of porous silicene with pores made in the form of either bi-, tri-, or hexavacancies as the active main material of the anode was proposed. Lithiation of the anode could be performed in both the horizontal and vertical directions. The external electric field acting on lithium ions in one direction or another was characterized by a strength of $E = 10^4$ V/m. The scheme for implementing both types of anode lithization in the model is shown in Figure 14. The case of vertical filling of the anode with lithium was nontrivial, as implemented in [48]. When using this filling option, the flow of lithium ions, which primarily fill the two-layer defective silicene, were directly perpendicular to its

surface. The silicon carbide film in this anode acts not only as a substrate, but also as a secondary active part of the anode. Initially, before lithium intercalation, the film had a wurtzite structure, as shown in Figure 14 [50]. The method of vertical filling of a silicene anode with lithium is gentler than the horizontal intercalation method [51].

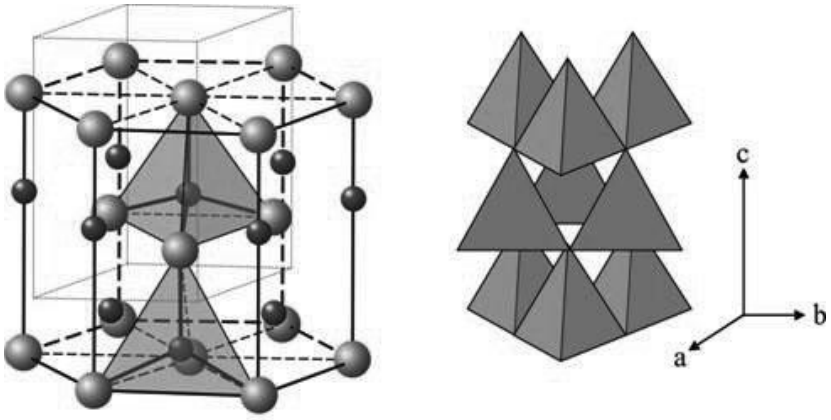

Figure 15. General view of the wurtzite structure (left) that the α-SiC modification of silicon carbide has; on the right, tetrahedral sites occupied by one of the types of atoms are highlighted and a system of coordinate axes is presented [50].

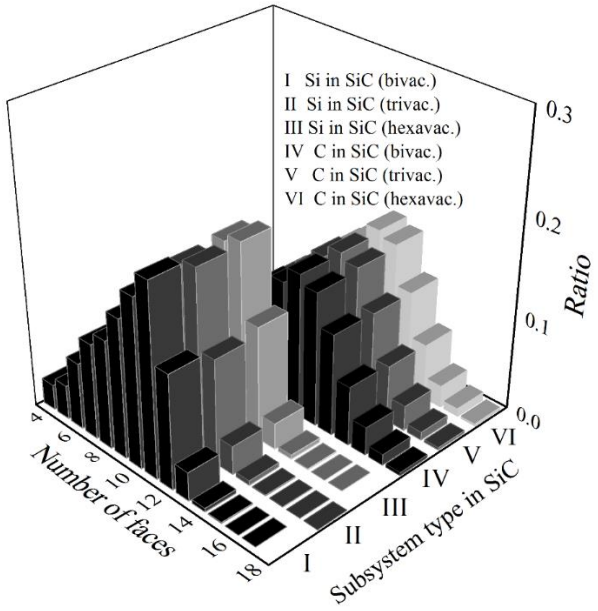

Figure 16. Distribution of Voronoi polyhedra by the number of faces, constructed for the "Si" and "C" subsystems of silicon carbide, after vertical filling of the "silicene/SiC" system with lithium for 1.51 ns. The type of defects in silicene is indicated in parentheses for the decoding of symbols [49].

The distribution of VP by the number of faces shows the quantitative composition of geometric neighbors (Figure 16). In the case of the Si subsystem, Si atoms are most often surrounded by 11

neighbors of the same type; for the C subsystem, C atoms are most often surrounded by 12 neighbors. The n distributions for the C subsystem extend to n = 18, while the extent of the corresponding distributions for the Si subsystem ends by n = 15. The mathematical expectations for the n spectra of the Si and C subsystems have a noticeable difference (on average by 20%). In this case, the asymmetries of the n distributions of the C and Si subsystems have opposite signs.

7. Modeling SiN_x thin film using kinetic Monte Carlo method

Silicon-nitrogen (SiN_x) films have a lower barrier to charge carrier injection than silicon oxide films. Due to their high carrier injection efficiency, these films are being increasingly used in nanoelectronic and optoelectronic devices. To obtain SiN_x films of the required thickness and quality, it is necessary to strictly control the microscopic random processes (e.g., adsorption, desorption, migration, and surface reactions) that occur during their growth [52]. Simulations allow us to explore many factors that influence film growth, such as substrate temperature. Kinetic Monte Carlo was used to simulate the evolution of the surface morphology of SiN_x thin films [53]. The processes of low-pressure chemical vapor deposition (LPCVD) of a porous SiN_x film using NH_3/Si_2H_6 gas flows were simulated. This process involved two microscopic processes: particle adsorption and surface migration.

In fact, only Si and N atoms participated in the deposition. The initial atomic matrix was filled with integers defining the type of atom: 0 - empty site, 1 - silicon adatom, and 3 - nitrogen adatom. New odd-layer particles deposited on the substrate were allowed to occupy alternating locations. In the even layer, other (different from the odd layer) positions were allowed for occupation. In each layer, alternating positions were observed for groups of Si and N atoms (Figure 17). In the resulting 3D model, a Si adatom of the perfect film had six nearest neighbors in the same horizontal layer and six nearest neighbors in both the bottom and top layers.

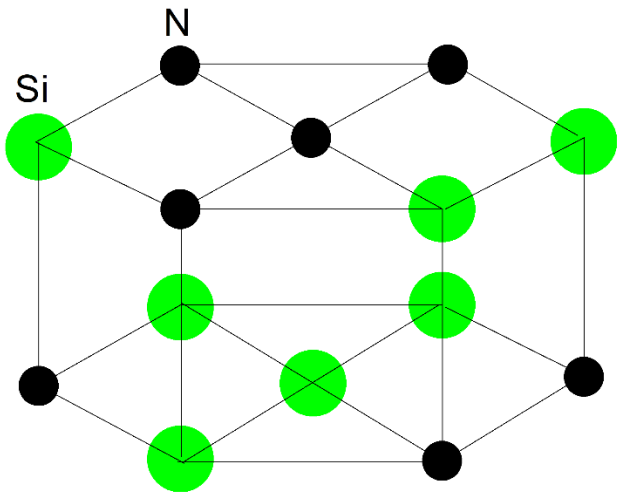

Figure 17. Scheme of occupation of Si and N atoms of discrete positions within the simulation lattice.

The total number of surface sites was 40,000. At each diffusion step, an initial location (x, y, z) of the atom was chosen at random. The deposited particle was shifted to its vacant neighboring site, thereby losing energy in the process. The atoms were deposited onto a silicon substrate. If an atom did

not immediately land on the substrate, it moved along the surface formed from the underlying deposited atoms until it reached the bottom of the stage, where it joined into a cluster of other adatoms. Before each new step, the probability of possible events was calculated. The generated random numbers determined the nature of the event (migration or deposition) to be performed. Such actions were carried out until the specified deposition time was reached. At the end of the calculation, the roughness of the resulting film was determined by numerical analysis. The described procedure was used to simulate changes in the surface morphology of SiN_x films. In the model, only Si and N atoms were directly deposited onto the substrate. Using different gas (Si and N) flow ratios, it was possible to achieve the necessary changes in the roughness and film thickness. Nitrogen at the deposition stage controlled the internal silicon nanostructure. The algorithm developed by the authors [52] allowed for the porosity, vacancies, and protrusions to be developed and, thus, created porous and rough films. The algorithm used did not allow small clusters of amorphous silicon to combine into larger clusters. It was shown that the surface amorphous Si clusters embedded in thin SiN_x films decreased in size when the gas flow increased. In this case, the film density increased.

8. Simulation of the deposition of silicon dioxide thin films

Modeling of a low-energy ion deposition process, such as ion-assisted deposition, was performed in [54] using the classical MD method. Such deposition can be carried out by thermal evaporation, with ion energies ranging from tens to hundreds of eV. The model is based on the presence of silicon and oxygen ions of two types: thermal, with an initial energy of 0.1 eV, and the assisting ions, with an energy of 100 eV and a charge of +1e. The charge parameters of oxygen (-0.65 e) and silicon (1.3 e) atoms were determined using the Takada potential [55]. The flow of silicon and oxygen ions was directed downward (i.e., perpendicular to the amorphous silicon substrate). The direction of the beam of assisting ions changed (i.e., they moved towards the substrate at different angles). The distance to which fast ions could approach film atoms was limited to 0.1 nm. Significant energies of the assisting ions required the use of a very small MD simulation step (0.05 fs). The simulation duration was 2 ps. Si and O atoms interacted directly on the substrate or on the surface of the resulting film, according to the Lennard-Jones potential. To perform this computer simulation, the GROMACS (Version 5.1.1) [56] program was used. Various parameters of the deposition process can have a strong influence on the structure, morphology, and properties of films [57]. The densest film without any visible anisotropy of the structure was obtained when high-energy assisting ions moved at an angle $\alpha = 60°$. By changing the flux density of the assisting ions, it was possible to regulate the stress in the resulting SiO_x film and to change its density within 0.5 g/cm^3.

9. Discussion

The modeling of physical processes is usually carried out with the aim of minimizing the experimental tests necessary to optimize these processes [58]. The studies discussed in this brief review were performed in the spirit of multiphysics modeling (i.e., the principles of physics, chemistry, and technology (in some cases) in a mathematical statement were considered) [59]. The advantages of electrodeposition modeling for predicting coating results are quite obvious [60,61]. For example, modeling elucidates that the potential of the surface electrode and the concentration of ions in the electrolyte affect the kinetics associated with the deposition process [62].

In the films obtained in the electrolytic deposition model both on silver and on graphite substrates, five-member rings formed by Si atoms could be traced. Such structural elements are also formed when vacancies are created in silicene [63]. If the five-link formations are not in the same plane, they can densely cover large areas without voids. Theoretically, it was shown that pentasilicene formed from pentagons alone retains many of the properties of ordinary hexagonal silicene [64].

Using the electrolytic deposition model of Si onto a graphite substrate, silicon islands with a 3D structure were obtained. Similar structures were observed in a physical experiment during the deposition of silicon on the highly oriented pyrolytic graphite (HOPG) under ultrahigh vacuum conditions [65]. The silicene obtained on HOPG was stable both at room temperature and at 350 °C. For electronics needs and for use in electrochemical devices, graphite-supported silicene is a cheaper option than silver-supported silicene [66]. In the model, polycrystalline silicon films with a large number of defects were obtained on both graphite and metal substrates. To obtain films with a more perfect crystal structure, a one-step electrodeposition process is likely to be insufficient and subsequent thermal annealing is required.

It has been experimentally shown that when van der Waals interactions exist between the film and the substrate, the presence of an impurity at the film growth front can contribute to the flat morphology [67]. For example, the addition of Cu to Ag influences the growth of a silver film on SiO_2. The advantage of a graphite substrate over a metal one is the fact that, due to lower adhesion, the transfer of silicene to the insulating substrate will proceed easier from the graphene substrate [68].

SiC is a wide bandgap semiconductor. The magnetic properties of the material formed by the SiC system alloyed with Ti, V, Cr, Mn, Fe, Co, Zn, Al, and Ge metals were investigated by the first-principles calculations [69]. The calculations revealed magnetic metals (SiC and Al-SiC), magnetic semiconductors with small magnetic moments (V-, Cr-, Mn-, Fe-, Co-, and Zn-SiC), and non-magnetic semiconductors (Ti- and Ge- SiC). The magnetic properties changed due to the filling of hybridization orbitals near the Fermi level, which are determined by the coupling of the 3d orbitals of transition metal atoms and defect states in the host material (SiC). The model observed a partial charge transfer from metal atoms to neighboring carbon atoms. The highest binding activity was observed in the Ti-SiC system. Stable bonds were formed between the transition metal Ti and neighboring C atoms.

The 4H-SiC modification of silicon carbide is used as a material for electromagnetic power devices. The magnitude of the avalanche breakdown field can serve as a criterion for the performance characteristics of this material. To assess the performance of power devices, the scaling theory was used. As proposed in [70], a quality indicator was introduced, which was a function of the avalanche breakdown field; this indicator was also considered as a unit measure of the power device performance. It was shown that the reduction in the avalanche breakdown voltage was facilitated by the anisotropy of the impact ionization coefficients, which appeared as an edge structural effect of the test material.

In general, molten salts have a large electrochemical window, which allows a large number of electrochemical processes to be carried out. The high decomposition potential and wide range of different salts, mixtures of salts, and salt eutectics with a wide range of temperatures make it possible to control various electrochemical reactions and their rates using temperature. Molten salts are divided into two categories: low-temperature (below 700 ˚C) and high-temperature (above 700 ˚C) salts [71]. Electrolysis is typically performed at a temperature ~100˚C above the melting point of the selected salt electrolyte. This allows for a reduction in the formation of associates when dissolving target products in the molten salt to speed up the electrochemical process. However, the use of high temperatures during electrolysis creates a problem with the selection of structural materials that can resist corrosion

in such aggressive environments.

The temperature of the deposition process can affect the diffusion properties of the growing material. Thus, in [72], using the example of platinum deposition on activated graphene with the formation of Pt nanoparticles on the substrate, it was shown that as the temperature increased, the priority shifted in favor of the individual atom's diffusion. In this case, the dependence of diffusion on the size of Pt particles disappeared. However, at lower temperatures depending on the particle size, dynamic coalescence predominated.

The influence of temperature on the crystallization of the deposited material occurs in different ways. At low temperatures, the proportion of critical clusters that ensure film growth increases. At the same time, due to an increase in the diffusion barrier, the rate of addition of new atoms to the cluster decreases. These processes illustrate that the size of the crystals decreases at low temperatures. As a rule, uniform film thickness is achieved with a uniform distribution of grains in the sediment [73]. Activation of the electrochemical system at a low temperature can be achieved through the use of an ultrasound.

The quality of deposited SiC crystals can be significantly improved via the optimization of the thermal regime [74]. In [75], the physical model of induction heating was considered and the growth process of SiC crystals was optimized; when subjected to optimization conditions, crystals with low defects were experimentally obtained. The simulation was carried out in the Virtual Reactor software package [76], where, based on mathematical models of heat transfer and mass transfer processes, it was possible to simulate the evolution of systems during the gas-solid crystal transition. Real processes were simulated, in which a SiC source was sublimated, led to the resulting vapor being transferred to a condensation zone, where it became saturated vapor, condensed, and turned into a crystal [77–79]. Due to the appropriate selection of thermal process parameters, an almost smooth, slightly convex growth boundary was realized in the model. Thus, a simple and feasible method was proposed to improve the quality of large-size SiC single crystals.

The correlation between deposition parameters and the resulting Si and SiC coating structures still remains an unresolved problem. To perform a targeted and effective optimization of the coating structure, a deeper understanding of the influence of the substrate temperature, deposition rate, and energy on the growing structure and mechanical properties of individual layers is required. This problem can be solved by MD simulations. This approach allows one to avoid labor-intensive and expensive experimental studies. For example, MD modeling makes it possibleto determine methods for nanometric grinding of single-crystalline Si, 4H-SiC and 6H-SiC [80], as well as to determine the region where the yield stress is violated near the Si/SiC and a-Si/SiC interfaces [81].

The increased use of silicon-containing products in the field of biomedicine, including therapeutic purposes [82], as well as the expansion of the use of electrochemical biosensors containing SiC materials [83], promotes a widespread implementation of MD studies in forecasting purposes.

10. Conclusions

MD models make it possible to reveal a picture of a complex phenomenon by synthesizing a large amount of information about a system into a single view. As our understanding of basic physical processes increases, so do the scale and complexity of the computer models used to describe them. The model usually includes simplifying approximations. Ultimately, these simplifications and even abstractions play a positive cognitive role. We understand which components of a system are

responsible for its specific behavior. Therefore, the model must reflect the essence of the phenomenon under study. In classical MD simulations, the most stringent requirements are posed on the interatomic potential used. In this regard, it is highly desirable to either repeat classical MD simulations using more accurate atomic interaction potentials or to perform simulations using other suitable methods. The choice of new research methods depends, to a large extent, on what can be sacrificed without significantly compromising the accuracy of the description of the modeled object or phenomenon. Thus, ab initio MD simulations can replace the corresponding classical simulation if the size of the system under study and the time of observation of the system are not critical parameters. Some assumptions can be checked within the framework of the same method. For example, during the MD deposition of Si^{4+} and C^{4+} ions onto various substrates, it would be possible to use a more accurate procedure for the appearance of these ions in the system. Although the production of thin films is achieved by different methods, the main focus is often on understanding the deposition process, and the optimization of properties is relegated to the background. For example, the structural properties of films receive a lot of attention, while properties such as the phase formation, chemical segregation, or stressation still remain poorly understood.

In biomedical applications, silicone material prove to be advantageous as compared with the other existing materials in the same field. The use of long-term implants has made silicone a widely recognized and biocompatible tool to the general public.

Use of AI tools declaration

The author declares he has not used Artificial Intelligence (AI) tools in the creation of this article.

Acknowledgments

This work was supported by Ministry of Science and Higher Education of the Russian Federation and is executed in the frame of the scientific theme of Institute of high-temperature electrochemistry UB RAS, number FUME-2022-0005, registration number 122020100205-5.

Conflict of interest

The author declares no conflict of interest.

References

1. Schoen FJ, Levy RJ, Tam H, et al. (2020) Pathological calcification of biomaterials, *Biomaterials Science*, 4 Ed., London: Elsevier, 973–994. https://doi.org/10.1016/B978-0-12-816137-1.00065-9
2. Sastri VR (2013) *Plastics in Medical Devices, Properties, Requirements, and Applications*, 2 Eds., Amsterdam: Elsevier. https://doi.org/10.1016/C2012-0-05946-7
3. Yesilirmak N, Altinors DD (2013) A silicone hydrogel contact lens after 7 years of continuous wear. *Cont Lens Anterior Eye* 36: 204–206. https://doi.org/10.1016/j.clae.2013.03.001
4. Saddow SE (2012) *Silicon Carbide Biotechnology: A Biocompatible Semiconductor for Advanced Biomedical Devices and Applications*, 1 Ed., Amsterdam: Elsevier. https://doi.org/10.1016/C2014-0-03629-5

5. Oliveros A, Guiseppi-Elie A, Saddow SE (2013) Silicon carbide: a versatile material for biosensor applications. *Biomed Microdevices* 15: 353–368. https://doi.org/10.1007/s10544-013-9742-3
6. Cruz RLJ, Ross MT, Powell SK, et al. (2020) Advancements in soft-tissue prosthetics part B: The chemistry of imitating life. *Front Bioeng Biotechnol* 8: 147. https://doi.org/10.3389/fbioe.2020.00147
7. Coletti C, Jaroszeski M, Pallaoro A, et al. (2007) Biocompatibility and wettability of crystalline SiC and Si surfaces. In: *Proceedings of the 29th Annual International Conference of the IEEE Engineering in Medicine and Biology Society*, Lyon, France, 5849–5852. https://doi.org/10.1109/IEMBS.2007.4353678
8. Saddow SE (2022) Silicon carbide technology for advanced human healthcare applications. *Micromachines (Basel)* 13: 346. https://doi.org/10.3390/mi13030346
9. Yunus G, Singh R, Raveendran S, et al. (2023) Electrochemical biosensors in healthcare services: bibliometric analysis and recent developments. *PeerJ* 11: e15566. https://doi.org/10.7717/peerj.15566
10. Jiang F, Liu Y, Yang Y, et al. (2012) Research progress of optical fabrication and surface-microstructure modification of SiC. *J Nanomater* 2012: 984048. https://doi.org/10.1155/2012/984048
11. Marsil N, Majlis BY, Mohd-Yasin F, et al. (2020) A review: properties of silicon carbide materials in MEMS application. *Int J Nanoelectron Mater* 13: 113–128. http://hdl.handle.net/10072/411838
12. Jani DB (2020) An overview on use of renewable solar energy in desiccant based thermal cooling systems. *J Algerian Studies* 1: 38–42. https://doi.org/10.5281/zenodo.4403022
13. Arvanitopoulos A, Antoniou M, Li F (2022) 3C-SiC-on-Si MOSFETs: Overcoming material technology limitations. *IEEE T Ind Appl* 58: 565–575. https://doi.org/10.1109/tia.2021.3119269
14. Toure M, Berenguier B, Kobor D (2018) Study by numerical simulation of a PN solar cell in 3C-SiC/Si. *Afr J Environ Sci Technol* 12: 532–537. https://doi.org/10.5897/AJEST2018.2565
15. Alkhaldi ND, Barman SK, Huda MN (2019) Crystal structures and the electronic properties of silicon-rich silicon carbide materials by first principle calculations. *Heliyon* 5: e02908. https://doi.org/10.1016/j.heliyon.2019.e02908
16. Lynch ME, Mebane D, Liu M (2010) Numerical continuum modeling and simulation of mixed-conducting thin film and patterned electrodes, *Ceramic Engineering and Science Proceedings*, 30: 129–138. https://doi.org/10.1002/9780470584316.ch12
17. Kang KH, Eun T, Jun MC, et al. (2014) Governing factors for the formation of 4H or 6H-SiC polytype during SiC crystal growth: An atomistic computational approach. *J Cryst Growth* 389: 120. https://doi.org/10.1016/j.jcrysgro.2013.12.007
18. Fiorentis E, Gatou MA, Lagopati N, et al. (2023) Biomedical applications of silica (SiO_2) nanoparticles. *J Sci Tech Res* 51: 42382–42389. https://doi. org/10.26717/BJSTR.2023.51.008057
19. Wei J, Ong PL, Tay FEH, et al. (2008) A new fabrication method of low stress PECVD SiN_x layers for biomedical applications. *Thin Solid Films* 516: 5181–5188. https://doi.org/10.1016/j.tsf.2007.07.051
20. Andersson H, van den Berg A (2003) Microfluidic devices for cellomics: a review. *Sens Actuators B: Chem* 92: 315–325. https://doi.org/10.1016/S0925-4005(03)00266-1
21. Lin Z, Chen K, Zhang P, et al. (2017) Improved power efficiency in phosphorus doped n-a-SiN_xO_y/p-Si heterojunction light emitting diode. *Appl Phys Lett* 110: 081109. https://doi.org/10.1063/1.4977419

22. Paviet-Salomon B, Gall S, Monna R, et al. (2011) Laser doping using phosphorus-doped silicon nitrides. *Energy Procedia* 8: 700–705. https://doi.org/10. 1016/j.egypro.2011.06.204
23. Arl D, Roge V, Adjeroud N, et al. (2020) SiO_2 thin film growth through a pure atomic layer deposition technique at room temperature. *RSC Adv* 10: 18073–18081. https://doi.org/10.1039/d0ra01602k
24. Gil-Ocaña V, Jimenez IM, Mayorga C, et al. (2021) Multiepitope dendrimeric antigen-silica particle composites as nano-based platforms for specific recognition of IgEs. *Front Immunol* 12: 750109. https://doi.org/10.3389/fimmu.2021.750109
25. Pandit B, Goda ES, Shaikh SF (2023) Electrochemical deposition toward thin films. In Sankapal, B.R., Ennaoui, A., Gupta, R.B., Lokhande, C.D., *Simple Chemical Methods for Thin Film Deposition*: *Synthesis and Applications*, Singapore: Springer, 245–304. https://doi.org/10.1007/978-981-99-0961-2-6
26. Yan Z, Liu R, Liu B, et al. (2023) Molecular dynamics simulation studies of properties, preparation, and performance of silicon carbide materials: a review. *Energies* 16: 1176. https://doi.org/10.3390/en16031176
27. Guan K, Zeng Q, Liu Y, et al. (2021) A multiscale model for CVD growth of silicon carbide. *Comp Mater Sci* 196: 110512. https://doi.org/10.1016/j.commatsci.2021.110512
28. Bhowmik S, Raian AG (2022) Chemical vapor deposition of 2D materials: a review of modeling, simulation, and machine learning studies. *Review* 25: 103832. https://doi.org/10.1016/j.isci2022.103832
29. Wu K, Mei Q, Liu H, et al. (2023) Vapor deposition growth of SiC crystal on 4H-SiC substrate by molecular dynamics simulation. *Crystals* 13: 715. https://doi.org/10.3390/cryst13050715
30. Ivanichkina KA, Galashev AY, Isakov AV (2021) Computational modeling of electrolytic deposition of a single-layer silicon film on silver and graphite substrates. *Appl Surf Sci* 561: 149959. https:/doi.org/10.1016/j.apsusc.2021.149959
31. Galashev AY, Abramova KA (2023) Computer simulation of obtaining thin films of silicon carbide. *Phys Chem Chem Phys* 25: 3834–3847. https://doi.org/10.1039/d2cp04208h
32. Laptev MV, Isakov AV, Grishenkova OV (2020) Electrodeposition of thin silicon films from the KF-KCl-KI-K_2SiF_6 melt. *J Electrochem Soc* 167: 04206. https://doi.org/10.1149/1945-7111/ab7aec.
33. Ewald P (1921) Die Berechnung optischer und elektrostatischer Gitterpotentiale. *Ann Phys-Berlin* 369: 253–287. https://doi.org/10.1002/andp.19213690304
34. Hockney RW, Eastwood JW (1988) *Computer Simulation Using Particles*, Philadelphia: Taylor & Francis. https://doi.org/10.1201/9780367806934
35. Yu R, Zhai P, Li G, et al. (2012) Molecular dynamics simulation of the mechanical properties of single-crystal bulk Mg_2Si. *J Electron Mater* 41: 1465–1469. https://doi.org/10.1007/s11664-012-1916-x
36. Foiles SM, Baskes MI, Daw MS (1986) Embedded-atom-methode functions for the fcc metals Cu, Ag, Au, Ni, Pd, Pt and their alloys. *Phys Rev B* 33: 7983. https://doi.org/10.1103/PhysRevB.33.7983
37. Tersoff J (1989) Modelng solid-state chemistry: Interatomic potentials for multicomponent systems. *Phys Rev B: Condens Matter Mater Phys* 39: 5566–5568. https://doi.org/10.1103/PhysRevB.39.5566.

38. Daw MS, Baskes MI (1984) Embedded-atom method: Derivation and application to impurities, surfaces, and other defects in metals. *Phys Rev B* 29: 6443. https://doi.org/10.1103/PhysRevB.29.6443
39. Finney JL (1979) A procedure for the construction of Voronoi polyhedral. *J Comput Phys* 32: 137–143. https://doi.org/10.1016/0021-9991(79)90146-3
40. Galashev AE, Skripov VP (1984) Investigation on the disordering of the argon hexagonal closed packed (HCP) crystals by the method of statistical geometry. *J Struct Chem* 25: 734–740. https://doi.org/10.1007/BF00747917
41. Galashev AE, Ivanichkina KA (2017) Computational study of the properties of silicon thin films on graphite. *Rus J Phys Chem A* 91: 2448–2452. https://doi.org/10.1134/S003602441712007X
42. Filatova EA, Hausmann D, Elliott SD (2018) Understanding the mechanism of SiC plasma-enhanced chemical vapor deposition (PECVD) and developing routes toward SiC atomic layer deposition (ALD) with density functional theory. *ACS Appl Mater Interfaces* 10: 15216–15225. https://doi.org/10.1021/acsami.8b00794
43. Daoud S, Bouarissa N, Rekab-Djabri H, et al. (2022) Structural and thermo-physical properties of 3C-SiC: high-temperature and high-pressure effects. *Silicon* 14: 6299–6309. https://doi.org/10.1007/s12633-021-01387-8
44. Thakur S, Dionne CJ, Karna P, et al. (2022) Density and atomic coordination dictate vibrational characteristics and thermal conductivity of amorphous silicon carbide. *Phys Rev Mater* 6: 094601. https://doi.org/10.1103/PhysRevMaterials.6.094601
45. Isakov A, Apisarov A, Khudorozhkova AO, et al. (2018) Electrodeposition of silicon onto copper substrate from KF-KCl-KI-K_2SiF_6 melt. *J Phys Conf Series* 1134: 012021. https://doi.org/10.1088/1742-6596/1134/1/012021
46. Deng J, Liu JZ, Medhekar NV (2013) Enhanced lithium adsorption and diffusion on silicene nanoribbons. *RSC Adv* 3: 20338–20344. https://doi.org/10.1039/C3RA43326A
47. Galashev AY, Abramova KA (2023) Molecular dynamics simulation of thin silicon carbide films formation by the electrolytic method. *Materials* 16: 3115. https://doi.org/10.3390/ma16083115
48. Galashev AY, Rakhmanova OR (2022) Two-layer silicene on the SiC substrate: lithiation investigation in the molecular dynamics experiment. *Chemphyschem* 23: e202200250. https://doi.org/10.1002/cphc.20220
49. Galashev AE (2023) Computer simulation of a silicene anode on a silicon carbide substrate. *Rus J Phys Chem B* 17: 113–121. https://doi.org/10.1134/S1990793123010190
50. Galashev AE (2022) Computer test of a silicene/silicon carbide anode for a lithium ion battery. *Rus J Phys Chem A* 96: 2757–2762. https://doi.org/10.1134/S0036024422120123
51. Rajapakse M, Karki B, Abu UO, et al. (2021) Intercalation as a versatile tool for fabrication, property tuning, and phase transitions in 2D materials. *NPJ 2D Mater Appl* 5: 30. https://doi.org/10.1038/s41699-021-00211-6
52. Bouhadiche A, Touam T (2018) Modeling and control of SiN_x thin film surface morphology using kinetic Monte Carlo method. *J Mater Sci* 6: 134–140. https://doi.org/10.4172/2321-6212.1000224
53. Bouhadiche A, Difellah Z, Bouridah H, et al. (2023) Modeling and control of SiN_x film growth using the kinetic Monte Carlo method: Impact of gas flow rate on surface roughness and film thickness. *Silicon* 15: 5209–5220. https://doi.org/10.1007/s12633-023-02415-5

54. Grigoriev FV, Sulimov VB, Tikhonravov AV (2022) Atomistic simulation of the ion-assisted deposition of silicon dioxide thin films. *Nanomaterials* 12: 3242. https://doi.org/10.3390/nano12183242
55. Takada A, Richet R, Catlow C (2004) Molecular dynamics simulations of vitreous silica structures. *J Non-Cryst Solids* 345–346: 224–229. https://doi.org/10.1016/j.jnoncrysol.2004.08.247
56. Abraham MJ, Murtola T, Schulz R, et al. (2015) GROMACS: high performance molecularsimulations through multi-level parallelism from laptops to supercomputers. *SoftwareX* 1–2: 19–25. https://doi.org/10.1016/j.softx.2015.06.001
57. Guo C, Kong M (2020) Fabrication of ultralow stress TiO_2/SiO_2 optical coatings by plasma ion-assisted deposition. *Coatings* 10: 720. https://doi.org/10.3390/coatings10080720
58. Dickinson EJF, Ekström H, Fontes E (2014) COMSOL Multiphysics®: Finite element software for electrochemical analysis. A mini-review. *Electrochem Comm* 40: 71–74. http://dx.doi.org/10.1016/j.elecom.2013.12.020
59. Datta A, Rakesh V (2009) *An Introduction to Modeling of Transport Processes*, Cambridge: Cambridge University Press. https://doi.org/10.1017/CBO9780511801150
60. Mandin P, Fabian C, Lincot D (2006) Importance of the density gradient effects in modelling electro deposition process at a rotating cylinder electrode. *Electrochim Acta* 51: 4067–4079. http://dx.doi.org/10.1016/j.electacta.2005.11.029
61. Hughes M, Strussevitch N, Bailey C, et al. (2010) Numerical algorithms for modelling electrodeposition: tracking the deposition front under forced convection from megasonic agitation. *Int J Numer Methods Fluids* 64: 237–268. http://dx.doi.org/10.1002/fld.2140
62. Mahapatro A, Suggu SK (2018) Modeling and simulation of electrodeposition: Effect of electrolyte current density and conductivity on electroplating thickness. *Adv Mater Sci* 3: 1–9. http://dx.doi.org/10.15761/AMS.1000143
63. Galashev AE, Ivanichkina KA (2019) Numerical simulation of the structure and mechanical properties of silicene layers on graphite during the lithium ion motion. *Phys Solid State* 61: 233–243. https://doi.org/10.1134/S1063783419020136
64. Wu D, Wang SW, Zhang SR, et al. (2019) Stabilization of two-dimensional penta-silicene for flexible lithium-ion battery via surface chemistry reconfiguration. *Phys Chem Chem Phys* 21: 1029–1037. https://doi.org/10.1039/c8cp05008b
65. Houssa M, Dimoulas A, Molle A (2015) Silicene: a review of recent of experimental and theoretical investigation. *J Phys: Condens Matter* 27: 253002. https://doi.org/10.1088/0953-8984/27/25/253002
66. Galashev AE, Ivanichkina KA, Vorobiyev AS, et al. (2017) Structure and stability of defective silicene on Ag(001) and Ag(111) substrates: a computer experiment. *Phys Solid State* 59: 1242–1252. https://doi.org/10.1134/S1063783417060087
67. Jamnig A, Pliatsikas N, Abadias G, et al. (1921) On the effect of copper as wetting agent during growth of thin silver films on silicon dioxide substrates. *Appl Surf Sci* 538: 148056. https://doi.org/10.1016/j.apsusc.2020.148056
68. Galashev AY, Vorob'ev AS (2020) Electronic and mechanical properties of silicene after nuclear transmutation doping with phosphorous. *J Mater Sci* 55: 11367–11381. https://doi.org/10.1007/s10853-020-04860-8

69. Zhang L, Cui Z (2022) First-principles study of metal impurities in silicon carbide: Structural, magnetic, and electronic properties. *Front Mater* 9: 956675. https://doi.org/10.3389/fmats.2022.956675
70. Kimoto T (2022) High-voltage SiC power devices for improved energy efficiency. *Proc Jpn Acad Ser B Phys Biol Sci* 98: 161–189. https://doi.org/10.2183/pjab.98.011
71. Ito Y, Nohira T (2000) Non-conventional electrolytes for electrochemical applications. *Electrochim Acta* 45: 2611–2622. https://doi. org/10.1016/S0013-4686(00)00341-8
72. Grillo F, Van Bui H, Moulijn JA, et al. (2017) Understanding and controlling the aggregative growth of platinum nanoparticles in atomic layer deposition: an avenue to size selection. *J Phys Chem Lett* 8: 975–983. https://doi.org/10.1021/acs.jpclett.6b02978
73. Mallik A, Ray BC (2011) Evolution of principle and practice of electrodeposited thin film: A review on effect of temperature and sonication. *Int J Electrochem* 2011: 8023. https://doi.org/10.4061/2011/568023
74. Zhang S, Fu H, Li T, et al. (2023) Study of effect of coil movement on growth conditions of SiC crystal. *Materials (Basel)* 16: 281. https://doi.org/10.3390/ma16010281
75. Zhang S, Fan G, Lic T, et al. (2022) Optimization of thermal field of 150 mm SiC crystal growth by PVT method. *RSC Adv* 12: 19936. https://doi.org/10.1039/d2ra02875a
76. Yang C, Liu G, Chen C, et al. (2018) Numerical simulation of temperature fields in a three-dimensional SiC crystal growth furnace with axisymmetric and spiral coils. *Appl Sci* 8: 705. https://doi.org/10.3390/app8050705
77. Ma RH, Zhang H, Ha S, et al. (2003) Integrated process modeling and experimental validation of silicon carbide sublimation growth. *J Cryst Growth* 252: 523–537. https://doi.org/10.1016/S0022-0248(03)00944-8
78. Manakov SM, Taurbavev NI (2012) Morphology and structural properties of *a*-Si:H and *a*-SiC:H films controlled in nanoscale. *J Nanoelectron Optoelectron* 7: 619–622. https://doi.org/10.1166/jno.2012.1402
79. Lebedev AA (1999) Deep level centers in silicon carbide: a review. *Semiconductors* 33: 107–130. https://doi.org/10.1134/1.1187657
80. Wang M, Zhu F, Xu Y, et al. (2018) Investigation of the differences in nanometric grinding of SiC and Si by molecular dynamics. In: *2018 International Conference on Electronics Packaging and iMAPS, All Asia Conference (ICEP-IAAC)*, Mie, Japan: IEEE. https://doi.org/10.23919/ICEP.2018.8374341
81. Samanta A, Grinberg I (2018) Investigation of Si/3C-SiC interface properties using classical molecular dynamics. *J Appl Phys* 124: 175110. https://doi.org/10.1063/1.5042203
82. Mazurek P, Vudayagiri S, Skov AL (2019) How to tailor flexible silicone elastomers with mechanical integrity: a tutorial review. *Chem Soc Rev* 48: 1448–1464. https://doi.org/10.1039/C8CS00963E
83. Li L, Li Y, Pei J, et al. (2023) Hotspots and trends of electrochemical biosensor technology: a bibliometric analysis from 2003 to 2023. *RSC Adv* 13: 30704–30717. https://doi.org/10.1039/D3RA05889A